https://doi.org/10.2298/SOS220610014T
Submitted: 10.06.2022.
Accepted for publication: 20.08.2022.
UDK: 069.51:549; 622.785

Application of pyrophyllite in high-temperature treated building materials

Anja Terzić[1,*], Milica V. Vasić[1], Jovica Stojanović[2], Vladimir B. Pavlović[3], Zagorka Radojević[1]

[1]Institute for materials testing - IMS, Bulevar vojvode Mišića 43, 11000 Belgrade, Serbia
[2] Institute for Technology of Nuclear and Other Mineral Raw Materials, Franchet d'Esperey 86, 11000 Belgrade, Serbia
[3]Faculty of Agriculture, University of Belgrade, Nemanjina 6, 11080 Belgrade

Corresponding author: anja.terzic@institutims.rs

Abstract:
Phyllosilicate mineral pyrophyllite is predominantly used in the ceramic industry because it exhibits high refractoriness. Due to its thermal transformation into mullite, pyrophyllite is stable at elevated temperatures, making it a suitable mineral additive for refractory non-shaped materials and various ceramic shaped products. In this study, pyrophyllite is employed as 50 % clay replacement in the ceramics and up to 30 % cement replacement in mortars. Physico-mechanical properties were investigated. The firing shrinkage in the ceramics treated at 1200 °C was reduced by pyrophyllite addition. Pyrophyllite acted as additional pozzolana during cement hydration. Within the microstructure, it formed micro-reinforcement in the shape of crystalline folia, which improves the mechanical properties of ordinary Portland cement, high aluminate cement, and blended cement mortars. The investigation proved the efficiency and suitability of pyrophyllite employed as a substitution for clay in ceramics and a cement replacement in mortars.

Keywords: Mineral additives; Sintering; Sustainable raw materials; Instrumental analyses.

1. Introduction

A layered hydroxy-aluminosilicate – pyrophyllite ($Al_2Si_4O_{10}(OH)_2$) is assembled of an Al octahedral sheet condensed between two tetrahedral Si sheets [1, 2]. Each Al atom in the octahedral 'module' shares four O atoms with adjoined Si tetrahedra. Additionally, Al atoms are bonded to two structural OH groups [1]. Being a 2:1 silicate, pyrophyllite exhibits limited substitution in the tetrahedral layers (upper limit of 7 % Al^{3+} in the tetrahedral sheet and 5 % Si^{4+} in the octahedral sheet) [1, 3]. This phyllosilicate mineral from the talc group is characterized by the softness of talc and its crystalline structure [4]. Pyrophyllite is highly resistant to acid attack due to the unstrained structure and the location of the O atoms merely between the layer surfaces [5]. The major customary impurities in the pyrophyllite ore are quartz, diaspore, bauxite, and mica. During heating, pyrophyllite loses the structural OH groups associated with its octahedral sheet (550°C) and forms mullite and cristobalite (1200°C) [6].

Pyrophyllite is an electrically neutral easily floatable raw material [7]. The application of high-energy milling upon standard ore refinement became a favorable procedure for pulverization and activation of the particles, structure destruction, and the extraction of targeted minerals [8, 9]. Due to its high effectiveness, milling is frequently adopted as an attainable option [10-15] even though mechanical activation is rarely an energetically sustainable choice. Pyrophyllite is mainly used in the field of refractories and ceramics due to

its good heat resistance, stable chemical properties, and crystal structure stability during heating. Here, pyrophyllite was employed without mechano-activation treatment to improve the cost-effectiveness of the high-temperature building materials processing.

The most recent studies are focused on themes such as the dissolution of pyrophyllite at elevated pressure conditions [16]. Large-scale quantum mechanical simulations of pyrophyllite dissolution provided an insight into the molecular mechanism of the process for phyllosilicate minerals far from equilibrium conditions. The overall reaction process comprises the sequence of reversible step-by-step elementary reaction events which change the denticity of the leaching surface group. Yuan et al. [17] investigated colloidal lead halide perovskite nanocrystals (NCs) which are versatile photonic sources. $CsPbX_3$ NCs were adsorbed on natural layered mineral pyrophyllite for improving heat, light, and water stability. The obtained materials were employed to fabricate white light-emitting diodes (WLEDs) with a wide color gamut of 117 %. Due to the swelling and cation-adsorbent properties of pyrophyllite, the dissolution of lead in water was significantly reduced, which plays a certain role in ecological protection. Ulian et al. [18] researched the interaction between water and a single layer of the (001) pyrophyllite surface. The results showed that water forms structures that resemble those typically found in the gas phase (water dimer and triangular cluster). The ab initio molecular dynamics simulations proved that this self-assembly is stable over the considered time. Sánchez-Soto et al. [19] investigated sintering behavior in the range of 800 – 1500°C of clay containing pyrophyllite, sericite, and kaolinite as ceramic raw materials. The thermally treated pyrophyllite-containing clay showed a dense network of rod-shaped and elongated needle-like crystals, being characteristic features of mullite. Qin et al. [20] investigated the thermodynamic and thermoelastic properties of pyrophyllite at high temperatures at the atomic scale. It was concluded that when pyrophyllite is used in the field of refractories, the particle size and amount of pyrophyllite should be reasonably selected to achieve the balance between the volume stability and strength of the material.

Extensive studies on the use of pyrophyllite in building materials are scarce and mostly limited to: utilization in ceramics as a replacement of quartz, clay, or feldspar [21-23], thermal transformation into mullite [24], or immobilization of toxic elements [25]. The application of pyrophyllite in mortar or concrete is seldom investigated [26]. In this study, pyrophyllite was used as substitutional raw material in ceramic (50 %) and mortars (10 %, 20 %, and 30 %). Physico-mechanical experiments were conducted. Hydration routes and the changes in the mineral composition and microstructure induced by pyrophyllite addition were monitored by instrumental techniques. The investigation aimed to prove the efficiency and suitability of pyrophyllite as a resource for the production of high-temperature treated building materials.

2. Materials and methods

2.1. Pyrophyllite

Pyrophyllite ore was issued from the deposit Parsovići, Bosnia and Herzegovina. A representative 300 kg sample was prepared in accordance with the standard ore sampling campaign [27]. After the rough crushing via jaw and cone crushers, the pyrophyllite ore was split into 10 kg sub-samples by cone and quartering method. Particle-size analysis of pyrophyllite sub-samples conducted by wet sieving on a set of W.S. Tyler test sieves is provided in Tab. I.

Tab. I Particle-size analysis of representative pyrophyllite sample.

Particle size/class, mm	M, %*	↓∑ M, %**	↑∑ M, %***
- 2.38 + 1.60	0.54	0.54	100.00
- 1.60 + 1.00	8.67	9.21	99.46

- 1.0 + 0.63	11.98	21.19	90.89
- 0.63 + 0.40	19.73	40.92	78.81
- 0.40 + 0.30	13.06	53.98	59.08
- 0.30 + 0.20	11.97	65.95	46.02
- 0.20 + 0.10	8.60	74.55	34.05
- 0.10 + 0.00	4.07	78.62	25.45

*The sum of the mass residues/oversize on sieves with mesh sizes 2.38 - 0.1 mm; **Mass residues/oversize on sieves with mesh sizes 2.38 - 0.1 mm; ***Mass undersize on sieves with mesh sizes 2.38 - 0.1 mm.

Chemical analysis of pyrophyllite was conducted by atomic absorption spectroscopy (AAS) technique on a PinAAcle 900 instrument (PerkinElmer). The samples were pulverized in a laboratory agate mill. The results are presented in Tab. II.

Tab. II Quantification of the major oxides in the pyrophyllite sample.

Oxide, %	SiO_2	Al_2O_3	Fe_2O_3	CaO	MgO	K_2O	Na_2O	TiO_2	SO_3	LoI*
Pyrophyllite	69.5	15.1	1.57	6.65	1.06	0.64	0.31	0.167	0.02	9.46

* Loss on ignition at 1000 °C

X-ray diffraction analysis of the pyrophyllite sample [4] highlighted pyrophyllite mineral as the most abundant phase counting up to approximately 50 % of all present crystalline phases. Quartz (≈30 %), calcite (≈10 %), and dolomite (≤5 %) were less abundant in the analyzed sample. Kaolinite was detected in traces.

2.2. Preparation of the experimental samples

2.2.1. Ceramic samples

Pyrophyllite (P) was mixed with three types of raw clays: 1) refractory clay from Crne Rovine (CR) deposit [28]; 2) ceramic clay from Gorne Crniljevo (GC) deposit [29]; and brick clay from Stalać (S) deposit. The chemical compositions of the clays were determined by EDXRF analysis on a Spectro Xepos system. The samples were pulverized in a vibratory mill. The results are given in Tab. III. Mix-design of the composite samples is provided in Tab. IV.

Tab. III Quantification of the major oxides in clay samples.

Oxide, %	SiO_2	Al_2O_3	Fe_2O_3	CaO	MgO	K_2O	Na_2O	TiO_2	MnO	P_2O_5	SO_3	LoI*
CR clay	56.85	25.70	2.47	0.44	0.91	1.55	0.56	1.21	0.02	0.07	0.07	10.15
GC clay	64.90	21.27	1.47	0.19	1.28	3.14	0.33	0.67	0.01	0.04	0.01	6.33
S clay	55.37	19.32	5.54	4.24	3.34	1.81	0.84	0.44	0.08	0.13	0.44	8.60

* Loss on ignition at 1000 °C

Tab. IV The mix-design of the ceramic samples.

Sample	P	CR clay	GC clay	S clay
P	100 %	-	-	-
PCR	50 %	50 %	-	-
PGC	50 %	-	50 %	-
PS	50 %	-	-	50 %

The experimental samples in form of semidry-pressed narrow tiles (25×120 mm) were prepared. Semidry pressing was conducted on a laboratory hydraulic press using dry raw materials mixed with 4 wt.% of distilled water and homogenized for 24 h.

Physico-mechanical experiments conducted on the ceramic specimens included: the determination of total carbonates content (volumetric method) [30], determination of residue on a 10,000 mesh/cm^2 (0.063 mm) sieve, plasticity, and sensitivity to drying [30]. The firing was conducted at 900 – 1300°C (heating rates: 70°C/h up to 200°C, 92°C/h up to 520°C, 60°C/h up to 610°C, and 140°C/h up to the final temperature with 1 h soaking). After the firing, loss on ignition, linear shrinkage (width and length), water absorption in boiling water, and three supports modulus of rupture was determined [29].

2.2.2. Mortar samples

Twelve mortars were prepared for the experiment. Ordinary Portland cement (OPC) - CEM I 42.5R Lafarge and high alumina cement (HAC) - Secar 71 were used as binders. Pyrophyllite was used as mineral addition and substitution for the binder. Andalusite was employed as aggregate (grain sizes 0.063 – 4.0 mm). The chemical composition of the raw materials was obtained by the AAS technique (Tab. V). Mix-design of the mortars is provided in Tab. VI.

Tab. V Quantification of the major oxides in the raw materials used for mortar samples.

Oxide, %	SiO_2	Al_2O_3	Fe_2O_3	CaO	MgO	K_2O	Na_2O	TiO_2	SO_3	LoI*
OPC	21.82	5.59	3.17	62.36	2.77	0.96	0.11	0	2.27	0.95
HAC	0.45	70.2	0.3	27.7	0.1	0.1	0.34	0	0.01	0.8
Andalusite	38.81	58.63	0.77	0.17	0.07	0.22	0.06	0.12	0.14	1.01

* Loss on ignition at 1000 °C

Tab. VI Mix-design of the experimental mortar samples.

Sample	OPC	HAC	Andalusite	Pyrophyllite
MAP	25 %	-	75 %	-
MAH	-	20 %	80 %	-
MAPH	15 %	15 %	70 %	-
MAP10	22.5 %	-	75 %	2.5 %
MAP20	20 %	-	75 %	5 %
MAP30	17.5 %	-	75 %	7.5 %
MAH10	-	18 %	80 %	2 %
MAH20	-	16 %	80 %	4 %
MAH30	-	14 %	80 %	6 %
MAPH10	13.5 %	13.5 %	70 %	3 %
MAPH20	12 %	12 %	70 %	6 %
MAPH30	10.5 %	10.5 %	70 %	9 %

Mortar samples were prepared according to the standard procedure [4, 31]. After 28 days, solidified mortar samples were fired in a laboratory furnace (temperature range 20 – 1000°C at a constant heating rate of 10°C/min).

2.3. Instrumental analyses

The XRD patterns were obtained on a Philips PW-1710 automated diffractometer using a Cu tube operated at 40 kV and 30 mA. The instrument was equipped with a diffracted beam curved graphite monochromator and a Xe-filled proportional counter. The diffraction data were collected in the 2θ Bragg angle range from 5 to 70 ^{o} counting for 1 s (qualitative identification) at every 0.02 ^{o} step. The divergence and receiving slits were fixed at 1 and 0.1. respectively. Measurements were performed at room temperature in a stationary sample holder.

Differential thermal analysis was conducted on the pulverized mortar samples (loose powder) using a SETSYS TG/DTA/DSC apparatus (SETARAM Instrumentation). Samples were placed in an alumina pan and heated from 20°C up to 1000°C. The heating rate was 10°C/min. The analysis was conducted in the static airflow.

The morphology of non-polished crushed mortar samples was analyzed on a JEOL JSM-6390 LV scanning electron microscope. The samples were covered with an Au film to improve the conductivity during recording.

3. Results and discussion

3.1. Ceramic samples

Plasticity and drying sensitivity of the ceramic samples P, PCR, PGC, and PS were

tested according to Pfefferkorn and Bigot, respectively [32]. The tests showed that all samples exhibited low to moderately plastic. As such, the samples are considered as non-susceptible to susceptible during the drying process. The lowest plasticity and, consecutively, sensitivity to drying were noticed in the pure pyrophyllite sample. The clay composites exhibited higher plasticity and sensitivity to drying.

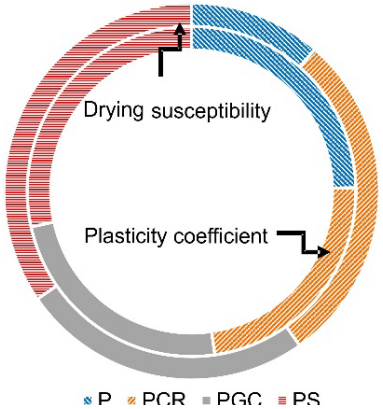

Fig. 1. Plasticity and drying susceptibility of P, PCR, PGC, and PS ceramic samples.

Loss on ignition (Fig. 2a) of the ceramic samples ranged from 7.13 to 9.17 %, predominantly showing a constant and mild increase with the increase of firing temperature. The highest LoI was noticed in the pyrophyllite (P) and PS samples due to the highest content of hydrated water and carbonates. The determined LoI values were higher than those of the usual floor ceramic tiles [29, 32], and rather similar to that of fired clay bricks [33].

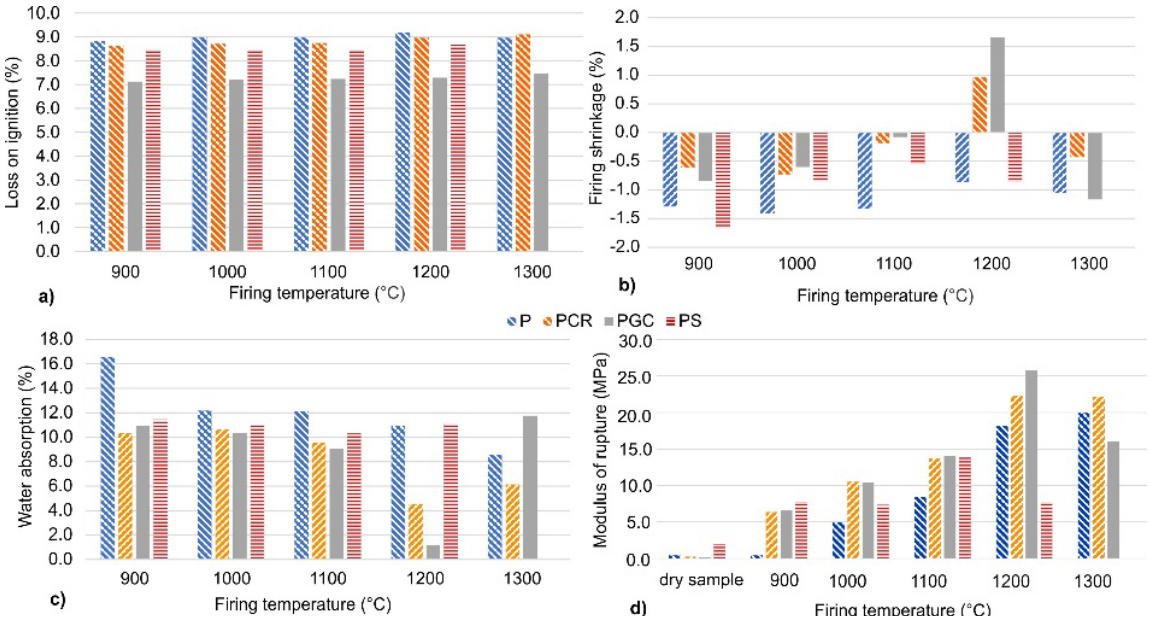

Fig. 2. Physico-mechanical characteristics: a) Loss on ignition, b) Firing shrinkage, c) Water absorption, and d) Modulus of rupture.

The firing shrinkage significantly decreased in comparison with the pure clay material (Fig. 2b). It showed generally undesirable behavior since most of the specimens underwent expansion. The highest expansion was noted in PS at the lowest firing temperature of 900°C, due to insufficient temperature for the complete reaction between carbonates and clay minerals [34]. The visible network of cracks appeared at the P sample`s surface at the same temperature, for the same reasons. The pyrophyllite samples expanded at all applied firing

temperatures due to the lower content of clay minerals when compared to the pure clays, and the presence of impurities [35, 36]. Therefore, using pyrophyllite in the ceramics can reduce the firing shrinkage, but the optimal firing regime and percent of addition have to be determined to avoid undesired cracking [35, 36].

Certain bulges occurred in the PCR and PGC samples upon firing at 1300°C due to the relatively abundant presence of organic matter and unreleased gas. A temperature of 1200°C can be considered high for the PS samples because excessive content of flux and the carbonates caused swelling. Therefore, PS samples were not fired at 1300°C. The optimal firing temperature according to this test is 1200°C, and the most favorable combinations were pyrophyllite with either refractory or ceramic clay (PCR and PGC).

The results and conclusions coincide with water absorption and modulus of rupture results (Figs. 2b and 2c). The water absorption test revealed that pyrophyllite alone could be used in wall ceramic tiles production. PCR and PGC can be utilized in the manufacturing of floor tiles fired at 1200°C [37]. All samples showed good characteristics upon firing at 900°C and 1000°C, and therefore they can be used in the production of fired bricks [38]. The PCR and PGC samples fired at 1200°C exhibited decreased water absorption in comparison with pure clays due to their intensified mullitization [39]. The mullitization process prevented a higher increase of the modulus of rupture from 1100°C to 1200°C in PGC and PCR samples. According to the standard-defined modulus of rupture [37], only the sample PCR complies with the ceramic tiles group, Annex J (water absorption between 3 and 6 %).

3.2. Mortar samples

Qualitative analyses of the mineral phase composition of MAP, MAH, MAPH, MAP20, MAH20, and MAPH20 mortars, conducted upon samples' curing for 28 days or after curing and subsequent firing at 1000°C (the samples marked with the label 1000) are presented in Figs. 3-5. After 28 days of hydration and solidification, all hydration reactions have been completed, the final mineral phase composition is established, and all mortars achieved at least 95 % of their projected mechanical strengths.

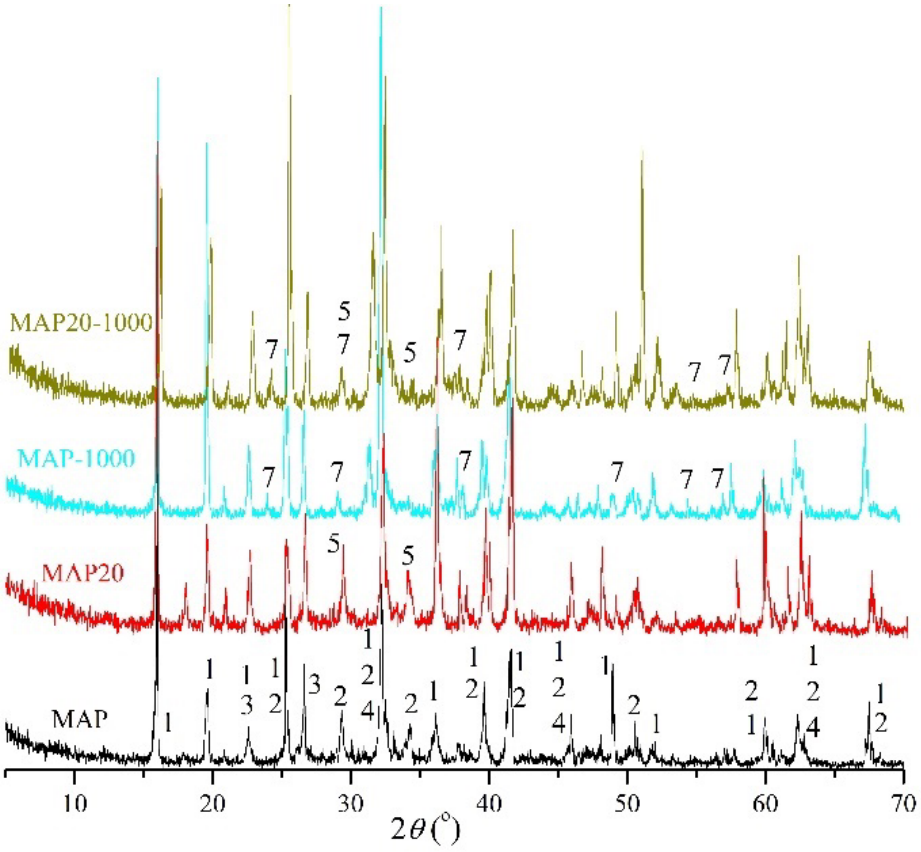

Fig. 3. XRD diffractograms of Portland cement mortars.

The phase composition of the MAP sample (Fig. 3) is: (1) Al_2SiO_5 (andalusite; JCPDS-39-0376[1]); (2) Ca_3SiO_5 (tricalcium silicate/alite; JCPDS-49-0442); (3) SiO_2 (quartz; JCPDS-46-1045); (4) Ca_2SiO_4 (dicalcium silicate/larnite (belite); JCPDS-77-0382). The most abundant phase is andalusite which originates from the aggregate share (75 %) in the mortar. Alite, which normally comprises 50 % of the total quantitative sum of cement minerals, is less abundant in this sample because the share of the cement was reduced to 25 wt.% to acquire a low-cement composite. Belite and quartz are present in smaller amounts. The well-defined crystalline peaks of cement minerals (i.e., Ca_3SiO_5, Ca_2SiO_4) point to the completion of the hydration reaction mechanisms [40]. Not all hydration products could be determined due to the intense overlapping and superposing of the minerals' peaks.

The MAP20 sample comprised the following mineral phases: 1) Al_2SiO_5 (andalusite); (2) Ca_3SiO_5 (alite); (3) SiO_2 (quartz); (5) $CaSiO_3$ (wollastonite; JCPDS-84-0655), and (6) $Ca_{12}Al_{14}O_{33}$ (mayenite; JCPDS-48-1882). Mayenite is a mesoporous calcium aluminum oxide with a characteristic crystalline structure. It is composed of interconnected cages with a positive electric charge per unit cell that includes two molecules $[Ca_{24}Al_{28}O_{64}]^{4+}$ and the remaining two "free" oxide ions O^{2-} that are trapped in the framework cages [41]. Mayenite, a product of cement hydration reactions due to the added pyrophyllite, is an excellent CO_2 sorbent. Presence of this phase implies on the possibility of using pyrophyllite as natural adsorbent and a means of immobilization of toxic elements and heavy metals present in mortar composition [42, 43]. The most abundant phase is andalusite. Alite, wollastonite, and

[1] Powder Diffraction File- number of the card. Joint Committee on Powder Diffraction Standards (JCPDS). Swarthmore. PA.

mayenite are less abundant. The major andalusite reflection at 15° was by 100 a.u.[2] higher than the corresponding reflection in the MAP sample due to the superposing of andalusite and alite reflection. Additional alite originates from hydration reactions that involve aluminum-oxide present in pyrophyllite [4, 46]. Larnite, a mineral that originates from a limestone portion in cement, was present in both investigated samples (MAP and MAP20). In cementitious materials, this mineral is usually referred to as belite. Belite contributes appreciably to strength at later ages. [40]. Wollastonite, with its acicular crystal structure, contributes to the good physical and mechanical properties of cementitious composite [45].

The identified phase composition of MAP-1000 (MAP sample after firing at 1000°C): (1) Al_2SiO_5 (andalusite), (3) SiO_2 (quartz), and (7) $Ca_2Al_2SiO_7$ (gehlenite; JCPDS-35-0755). Gehlenite ($Ca_2Al[AlSiO_7]$) is a mineral stable at high temperatures – up to 1593°C [46]. In OPC based mortar, gehlenite occurred as a product of reactions between cement minerals induced by thermal treatment. With the increase in the sintering temperature, the crystallinity of the gehlenite mineral significantly improves, as well as the compressive strength of the mortar; therefore, these cement minerals contribute to the mechanical properties of Portland cement-based mortar [47].

The phase composition of MAP20-1000 is: (1) andalusite, (3) quartz, (5) wollastonite and (7) gehlenite. The content of gehlenite is much higher in comparison to the MAP-1000 samples which can be related to the pyrophyllite addition.

MAH sample (Fig. 4) comprised: (1) Al_2SiO_5 (andalusite); (3) SiO_2 (quartz); (4) Ca_2SiO_4 (larnite/belite); and (5) $CaSiO_3$ (wollastonite). The most abundant phase is andalusite, while all other phases are less abundant. Tricalcium aluminate (C_3A) and monocalcium aluminate ($CaO{\cdot}Al_2O_3$), which are the main constituent of hydrated high aluminate cement, are overlapped and superposed with andalusite peaks in the XRD diffractogram [48]. Thereby, the main andalusite reflections in the MAH sample located at 15°, 33°, and 42° are by 100, 400, and 200 arbitrary units, respectively, (Fig. 4) higher than the corresponding reflections in the MAP sample (Fig. 3). The previous statement is explained by the different hydration mechanisms of OPC and HAC [49]. In addition, tricalcium silicate was identified in the MAP sample as a typical product of the Portland cement hydration. It was not present in MAH mortar due to differences in hydration route between Portland and high-aluminate cement [49].

[2] a.u. are arbitrary units for approximate quantification of XRD diffractograms [4]

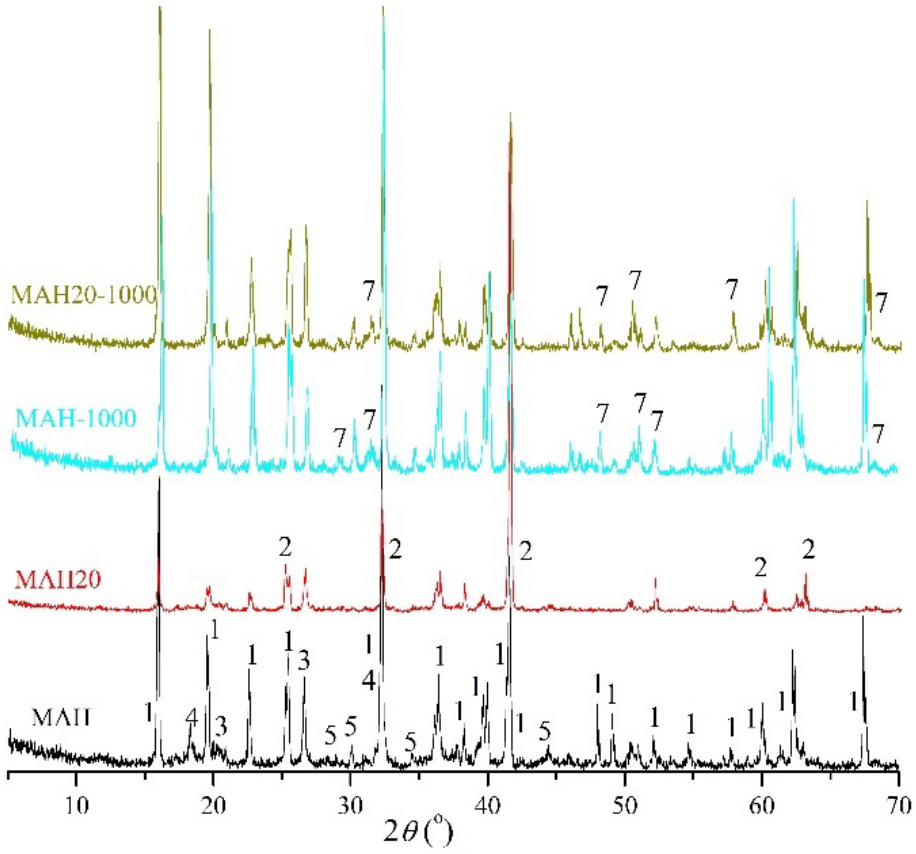

Fig. 4. XRD diffractograms of high-aluminate cement mortars.

The crystalline phases present in the MAH20 sample are: (1) andalusite; (2) alite, and (3) quartz. The crystallinity degree of all present phases is noticeably higher in comparison to all other samples. The reflection at 42° is exceptionally prominent, probably due to C_3A formation triggered by the presence of pyrophyllite addition [44]. Due to intense overlapping and superposing of Al_2SiO_5 and C_3A reflections, tricalcium aluminate cannot be quantified. Tricalcium silicate is present in this refractory mortar due to reactions between HAC and the pyrophyllite addition.

The MAH-1000 sample comprises (1) andalusite, (3) quartz, (5) wollastonite, and (7) gehlenite, which is a mineral composition similar to that of OPC-based mortar (MAP) after thermal treatment at 1000°C. Thereby, a mortar with OPC used a bonding agent and andalusite as aggerate can be employed at working temperatures of 1000°C same as a mortar designed with the refractory binder.

Andalusite (1), quartz (3), wollastonite (5), and gehlenite (7) were identified in the MAH20-1000 sample same as in the MAH-1000. Visual determination of the crystallinity degree of the mineral phases present in these two samples highlights insignificant differences between the corresponding peaks (i.e., peaks of the same mineral phases identified in these two mortars). Namely, pyrophyllite contributes more to the crystallinity of Portland cement-based mortar, while in the HAC-based mortar, the pyrophyllite addition brings no noteworthy changes. Additionally, pyrophyllite, a refractory raw material, contributes more to the thermal resistance of Portland cement composite (customarily considered a non-refractory material) than to mortar based on refractory cement. Thereby, pyrophyllite can be used as an additional refractory resource, enhancing the thermal resistance of non-refractory mortars.

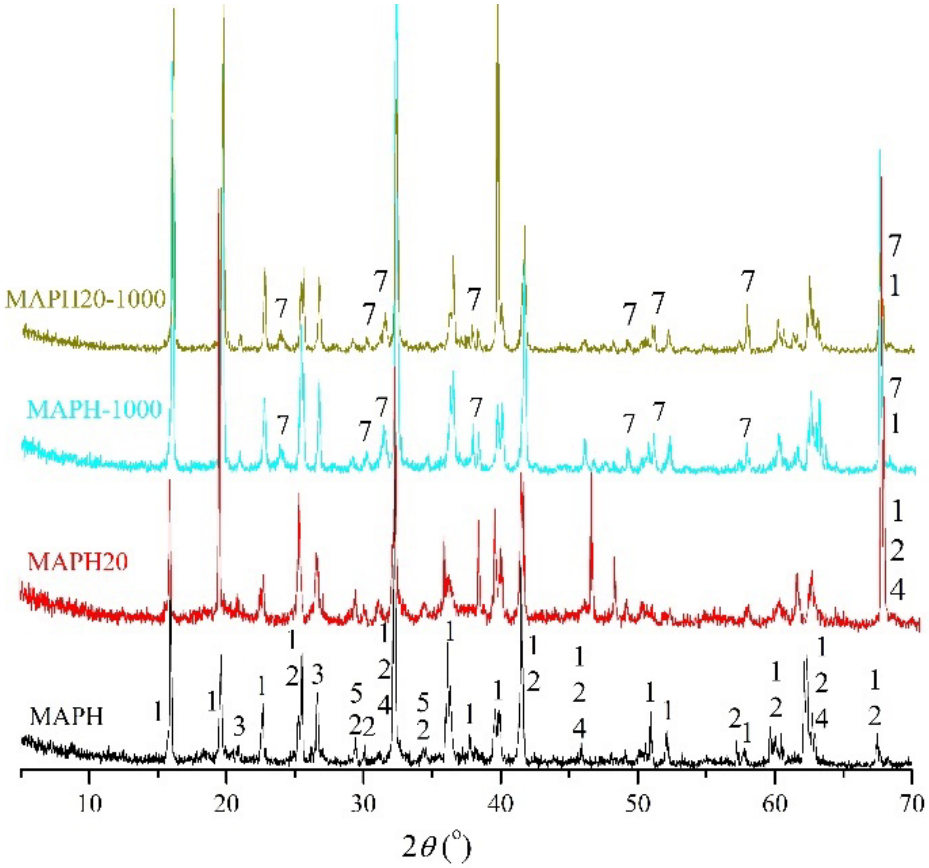

Fig. 5. XRD diffractograms of blended cement mortars.

The phases identified in the MAPH sample (Fig. 5) are: (1) Al_2SiO_5 (andalusite); (2) Ca_3SiO_5 (alite); (3) SiO_2 (quartz); (4) Ca_2SiO_4 (belite); and (5) $CaSiO_3$ (wollastonite). The most abundant phase is andalusite. Ca_3SiO_5 is less abundant than in the MAH sample due to the smaller quantity of the OPC in the blended biner. Wollastonite, belite, and quartz are less abundant than andalusite. Regarding the intensity of crystalline reflections, the MAPH sample is between approximate values identified for MAP and MAH samples because this mortar comprises a blend of two types of cement – OPC and HAC [49, 50].

Andalusite (1); tricalcium silicate (2); quartz (3); belite (4); and wollastonite (5) are present in the MAPH20 sample. The MAPH20 crystallinity is higher than that of MAP20 but lesser than MAH20. Also, in comparison with the MAPH mortar, MAPH20 exhibited more intense peaks at 20° and 70° due to the contribution of pyrophyllite minerals to the reactions taking place within the bonding agent based on the blend of two types of cement [4, 44].

The MAPH-1000 sample consists of (1) andalusite, (3) quartz, (5) wollastonite, and (7) gehlenite. The crystalline peaks of all present phases are significantly higher than in the MAPH sample. Gehlenite develops as a product of thermally induced reactions between OPC minerals. On the other side, wollastonite – an outcome of interactions among high alumina cement minerals contributed to the overall crystallinity of the MAPH-1000 sample. The presence of minerals with a high melting point, such as gehlenite and wollastonite, indicates good refractoriness of this mortar.

MAPH20-1000 comprises the same mineral phases as the MAPH-1000. The difference between intensities of analogous mineral reflections in these two samples is indistinguishable. In this case, the pyrophyllite addition contributed more to the hydration process than to the sintering of the sample with a blended cement binder.

Hydration mechanism and thermal changes of mortar samples were observed by

differential thermal analysis accompanied by thermogravimetry. The diagrams are in Fig. 6.

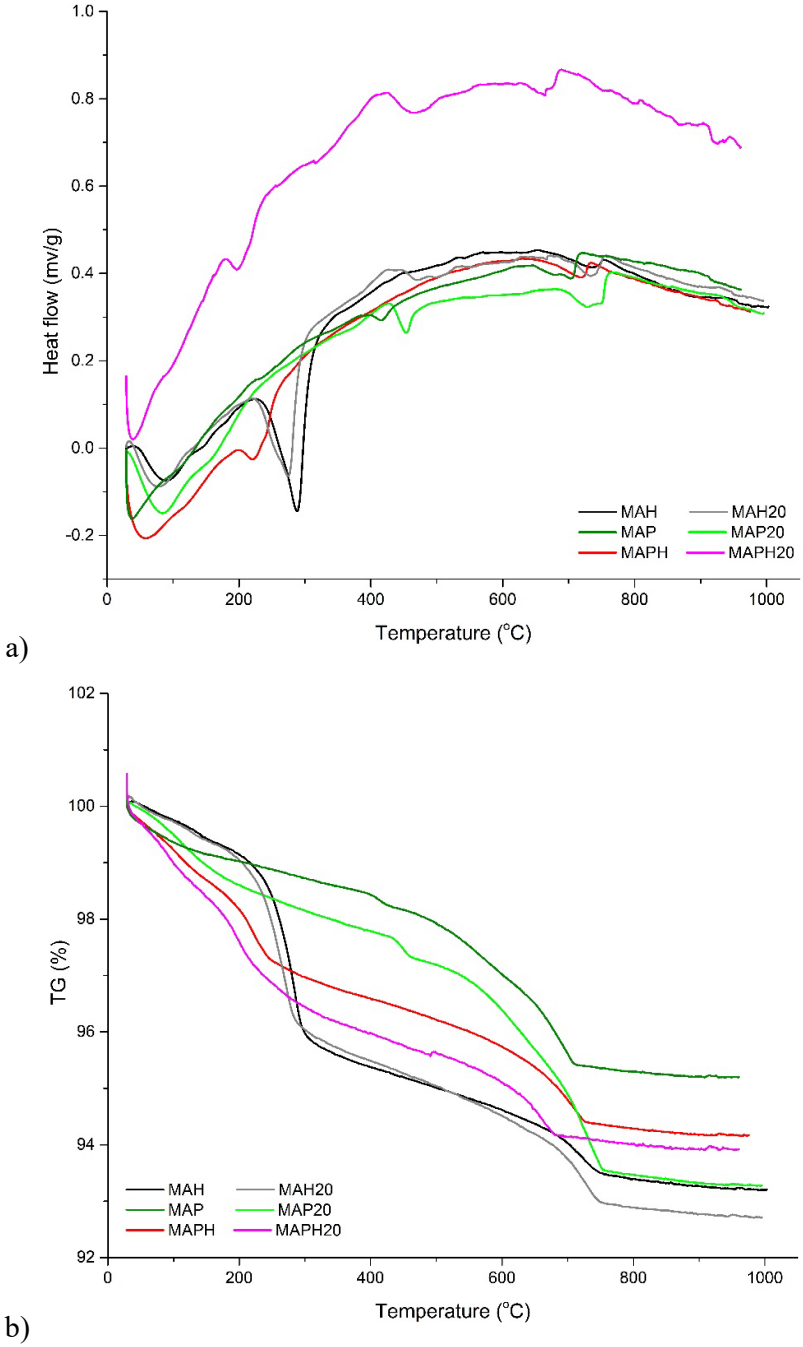

Fig. 6. Thermal curves of the mortar samples obtained by: a) DTA; b) TGA.

The initial effects registered by DTA (Fig. 6a) were set below 100°C. These endothermic peaks were well defined in each diagram. The maxima were identified at 50°, 95°, 98°, 93°, 75°, and 54°C for MAP, MAP20, MAH, MAH20, MAPH, and MAPH20, respectively. Besides the loss of water, the initial effects are usually associated with the dehydration of $AH_3 \cdot H_2O$ gel, which takes place at approximately 120°C, and the formation of ettringite and colloidal C-S-H gel (100–150°C) [4]. The pyrophyllite addition delayed these reactions in OPC mortars while it accelerated the rate of reactions in the blended mortars. In HAC mortars, the pyrophyllite addition did not affect the reactions below 200°C.

The peak identified at approximately 300°C for MAH (296°C) and MAH20 (301°C) is related to monocalcium aluminate ($CaAl_2O_4$). This HAC mineral reacts with water forming the metastable hydrate $CaO{\cdot}Al_2O_3{\cdot}10H_2O$, or a mixture of $2CaO{\cdot}Al_2O_3{\cdot}8H_2O$, $3CaO{\cdot}Al_2O_3{\cdot}6H_2O$ and $Al(OH)_3$ gel. These reactions form the first stage of strength development in calcium aluminate cement [51]. The pyrophyllite addition did not significantly change the hydration mechanism of the HAC-based sample at 300°C.

The following effects on the DTA were noticed in the 450-500°C vicinity. The reactions at this temperature are usually associated with the decomposition of cement's aluminate phase $C_{12}A_7$ [4]. Depending on additives, the dehydration of the calcium aluminate and alumina hydrates is near completion at 500°C, which is usually associated with an endothermic effect on a DTA curve [4]. The endothermic maxima for MAP and MAP20 were 427° and 475°C, respectively. The pyrophyllite addition postponed this reaction. MAH and MAH20 did not exhibit any effect at this thermal interval. MAPH and MAPH20 showed exothermal peaks at 441°C and 424°C, which means that in mortars with blended cement, the pyrophyllite addition accelerated this reaction. The effects above 500°C can partially correlate to the α- to β-quartz polymorphic transformation. These effects are superposed with the effect caused by the calcination of calcite typically completed at 890°C. Also, pyrophyllite mineral shows a broad endothermic dehydration peak centered at 760°C and a shoulder effect at 840°C, the latter being associated with a residual loss of hydroxyl groups [4], in accordance with DTA diagrams in Fig. 6a. The differential thermal analysis highlighted that pyrophyllite did not negatively interfere with the cement hydration route; moreover, this mineral additive behaved as pozzolana.

The total mass loss registered in the 20 – 1000°C interval on the TGA curves (Fig. 6b) summed up to 4.5, 6.8, 7, 7.3, 5.6, and 6 % for MAP, MAP20, MAH, MAH20, MAPH and MAPH20, respectively. HAC-based mortars experienced the most significant mass loss. MAP mortar showed the slightest mass change. Pyrophyllite addition induced higher mass loss in all mortar samples. The changes on the TGA curves of MAP, MAP20, MAPH, and MAPH20 that occurred in the 20 – 420°C interval are related to the release of evaporable water and part of the bound water (30 – 105°C), the dehydration of C-S-H gel (120 – 240°C), and portlandite dehydroxylation (240 - 420°C) [4]. MAH and MAH20 samples exhibited huge mass loss at 300°C due to the monocalcium aluminate reaction with water, which follows DTA results. The mass loss registered in all samples from 600°C to 800°C can be correlated to the $CaCO_3$ decomposition (at approximately 700°C). Since pyrophyllite comprised about 10 % of calcite and an additional 5 % dolomite in mineral composition, this effect on the TG curve was more pronounced in the samples with pyrophyllite addition.

The parts of the crushed mortar samples MAP, MAH, MAPH, MAP20, MAH20, and MAPH20 were recorded using a scanning electron microscope. The microstructure of fully hydrated and solidified mortars, composed of a cement matrix closely merged with andalusite aggregate grains, can be seen in Fig. 7a-f. All samples are well consolidated with a very low visible porosity. Present pores are small and round (as seen in Fig. 7b and 7e). No formed clusters of voids are detected. No increased porosity in the cement-aggregate transition zone is present, which usually refers to good mechanical performance, i.e., high mechanical strengths of mortar [4, 43].

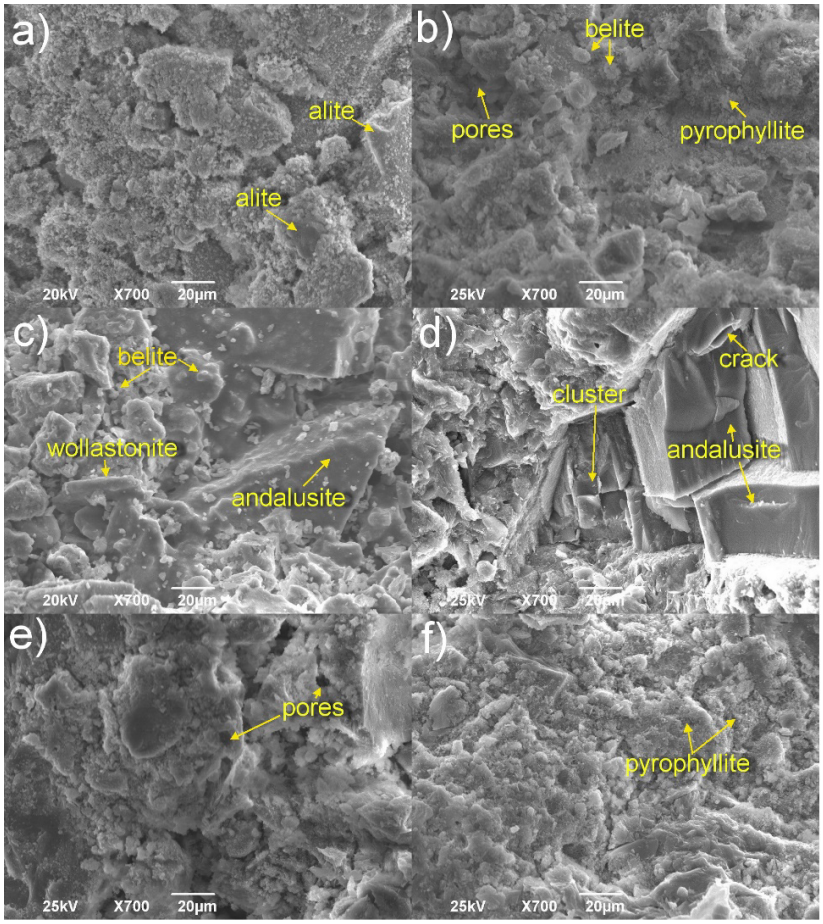

Fig. 7. SEM microphotographs of the mortar samples: a) MAP; b) MAP20; c) MAH; d) MAH20; e) MAPH, and f) MAPH20.

Andalusite grains composed of blocky prismatic crystals with sharp edges are visible in the microphotographs of the MAH and MAH20 samples (Fig. 7c and 7d). Andalusite is an aluminum silicate mineral of metamorphic origin. It crystallizes in an orthorhombic system and forms euhedral, pseudo-tetragonal columnar crystals with good fissility parallel to the plane (110) and slightly poorer along a plane (100) [52]. Andalusite has a chemical composition of 63 % Al_2O_3 and 37 % SiO_2, but it usually contains impurities (for example, carbon) [53]. The mineral inclusions (isotropic aggregates) occur around or within microstructural defects, i.e., microcracks and cracks, scattered on the surface of andalusite grains [54]. The crack in the andalusite grain is visible in Fig. 6c. Andalusite crystals are either single or merged into clusters [54] as seen in Fig. 7d.

The cement matrix is composed of very small particles belonging to various cement minerals. According to the XRD analysis, the particles in the MAP sample's cement matrix (Fig. 7.) primarily correspond to alite and belite. Alite crystals are mostly thick and relatively prismatic but with moderately rounded edges, sizing approximately 20 - 30 μm (Fig. 7a). Belite crystals are blocky but gritty and comparatively smaller [56, 57]. In Fig. 6b, belite minerals are visible as round-shaped tiny formations of approximately 5 μm diameter positioned on the top of larger alite particles. Alite particles are closely merged into clusters of various minerals (Fig. 7a). Upon 28 days of hydration and solidification, a cementitious material comprises relatively uniform overlapped mineral clusters packed randomly together [58].

The MAH sample (Fig. 7c) is relatively rich in belite and wollastonite. Wollastonite

occurs as a flat elongated (knife-like) crystal mass. Single crystals of wollastonite are acicular, i.e., needle-like [59]. In particular, characteristic white-colored wollastonite crystals are visible on top of the bigger andalusite particles in the microphotograph of the MAH sample (Fig. 7c).

The influence of pyrophyllite addition on the mortar microstructure can be observed in Figs. 7b and 7f. Namely, the clusters of cement minerals merged with andalusite grains as well as the entire space between grains are now filled and covered with very small needle-like formations. These so-called crystalline folia are characteristic for pyrophyllite [4]. Thereby, they provide a sort of micro-reinforcement for the composite microstructure, improving the mortar's mechanical properties.

The pyrophyllite addition makes a higher impact on the performances of mortars based on ordinary Portland cement. It is assumed that the optimal physico-mechanical properties will be obtained for mortars with addition of pyrophyllite up to 20 %.

4. Conclusion

Pyrophyllite was successfully employed as a 50 % replacement resource in the refractory, ceramic, and carbonate raw clay composites, as well as up to 30 % replacement in mortars based on andalusite, ordinary Portland cement, and high aluminate cement. The investigation proved the efficiency and suitability of pyrophyllite as a resource for producing high-temperature processed building materials.

In ceramics, pyrophyllite reduced the firing shrinkage, but the optimal firing regime and percent of addition must be further tested to avoid undesired cracking. The recommended firing temperature is 1200°C. The composites with the best performances were pyrophyllite with either refractory or ceramic clay to manufacture floor tiles fired at 1200°C. Pyrophyllite can solely be used in wall tiles production.

In mortars, pyrophyllite contributed to the hydration of ordinary Portland cement as it propagated the additional quantity of mineral phases (alite, belite, wollastonite, and gehlenite), which influenced the increase in compressive strength and refractoriness of Portland cement-based mortars. This influence was less notable in high aluminate cement mortars, while in blended cement mortars, the result was moderate. Crystalline folia, characteristic of pyrophyllite, was detected, forming the micro-reinforcement within the mortar's microstructure. Pyrophyllite addition of up to 20 % can be used in building or refractory mortars (fired at 1000°C) without deterioration of their performances.

Acknowledgements

This investigation is financially supported by the Ministry of Education, Science and Technological Development of the Republic of Serbia (Contract No.: 451-03-68/2022-14/ 200012). The authors would like to express gratitude to dr. Smilja Marković (Institute of Technical Sciences of SASA, Serbia) for conducting the DTA analysis. Also, the authors would like to thank colleagues from the Institute for Technology of Nuclear and Other Mineral Raw Materials for providing pyrophyllite for the experiment.

5. References

1. S. Mohammadnejad, J. Provis, J. van Deventer, Hydrometallurgy 146 (2014) 154.
2. R. Wardle, G.W. Brindley, Am. Mineral. 57 (1972) 732.
3. J. Temuujin, K. Okada, T. Jadambaa, K. MacKenzie, J. Amarsanaa, J. Eur. Ceram. Soc. 23 (2003) 1277.
4. A. Terzić, D. Radulović, M. Pezo, J. Stojanović, L. Pezo, Z. Radojević, Lj. Andrić, Constr. Build. Mater. 258 (2020) 119721.
5. C. Maqueda, J.L.P. Rodríguez, A. Justo, Analyst 112 (1987) 1085.
6. P.J. Sánchez-Soto, A. Justo, J.L. Pérez-Rodríguez, J. Mater. Sci. 29 (1994) 1276.

7. K. Zhao, W. Yana, X. Wang, B. Hui, G. Gu, H. Wang, Int. J. Miner. Process. 161 (2017) 78.
8. T. Alex, R. Kumar, S. Roy, S. Mehrotra, Miner. Process. Extr. Met. Rev. 37 (2016) 1.
9. Q. Tan, C. Deng, J. Li, J. Clean. Prod. 142 (2017) 2187.
10. L. Maqueda, O. Montes, E. Macias, F.Franco, J. Poyato, J. Rodrıguez, Appl. Clay. Sci. 24 (2004) 201.
11. J. Rodríguez, L. Sanchez del Villar, P. Sanchez-Soto, Clay Miner. 23 (1988) 399.
12. U. Caligulu, H. Durmus, M. Akkas, B. Sahin, Sci. Sint. 53 (2021) 475.
13. M. Erdemoglu, M. Birinci1, T.Uysal, E. Porgalı Tuzer, T. Saidou Barry, J. Mater. Sci. 53 (2018) 13801.
14. A. Wiewiora, P Sanchez-Soto, M.Aviles, A. Justo, J.Rodriguez, Appl. Clay Sci. 8 (1993) 261.
15. J. Filio, K. Sugiyama, F. Saito, Y. Waseda, Int. J. Soc. Mat. Eng. Res. 1 (1993) 140.
16. R. Schliemann, S. Churakov, Geochimica et Cosmochimica Acta 307 (2021) 42.
17. L. Yuan, Y. Zhou, Z. Wang, E. Mei, X. Liang, W. Xiang, Appl. Clay Sci. 211 (2021) 106158.
18. G. Ulian, D. Moro, G. Valdr, Appl. Clay Sci. 212 (2021) 106221.
19. P. J. Sánchez-Soto, E. Garzón, L. Pérez-Villarejo, D. Eliche-Quesada, Boletín de la Sociedad Española de Cerámica y Vidrio (2021) https://doi.org/10.1016/j.bsecv.2021.09.001
20. X. Qin, J. Zhao, R. Wei, Y. Cao, M. He, Physica B: Condensed Matter 625 (2022) 413513.
21. S. Amritphale, S. Bhasin, N. Chandra, Ceram Int 32 (2006) 181.
22. N. Ismail, N. Kamilah Saat, M. Hafiz, M. Zaid, Sci. Sint. 53 (2021) 509.
23. R. Sule, I. Sigalas, Appl. Clay. Sci. 162 (2018) 288–296.
24. P. Sanchez-Soto, A. Justo, J.Rodriguez, J. Am. Ceram. Soc. 72:1 (1989) 154.
25. K. Shiota, T. Nakamura, M. Takaoka, J Environ. Manag. 201 (2017) 327.
26. R. Anggraini, R. Ristinah, S. Budio, Rekayasa Sipil 7:3 (2014) 210.
27. J.W. Merks, Sampling and weighing of bulk solids: Trans Tech, Clausthal-Zellerfeld, Germany, 1985.
28. M. Arsenović, L. Pezo, S. Stanković, Z. Radojević, Ceram. Int. 39(6) (2013) 6277.
29. M. V.Vasić, L. Pezo, M. R.Vasić, N. Mijatović, M. Mitrić, Z. Radojević, Boletín de la Sociedad Española de Cerámica y Vidrio (2020) https://doi.org/10.1016/j.bsecv.2020.11.006.
30. M. Arsenović, S. Stankovic, L. Pezo, L Mancic, Z. Radojevic, Ceramics International 39 (2013) 3065
31. A. Terzić, M. Dojčinović, Lj. Miličić, J. Stojanović, Z. Radojević, Sci. Sint. 53 (2021) 445.
32. M. V. Vasić, N. Mijatović, Z. Radojević, Materials 15(9) (2022) 3145.
33. M. V. Vasić, G. Geol, M. Vasić, Z. Radojević, Environ. Technol. Innovation 21 (2021) 101350. 10.1016/j.eti.2020.101350
34. C. Tschegg, T. Ntaflos, I. Hein, Appl. Clay Sci. 43(1) (2009) 69.
35. T.K. Mukhopadhyay, S. Ghatak, H.S. Maiti, Ceram. Int. 36(3) (2010) 909.
36. I. E. Sproat, J. Am. Ceram. Soc. 19 (1936) 135.
37. SRPS EN ISO 14411:2015. Ceramic tiles - Definitions, classification, characteristics, evaluation of conformity and marking
38. S. Iftikhar, K. Rashid, E. U. Haq, I.Z. Fahad, K. Alqahtani, M. I. Khan, Constr. Build. Mater. 259 (2020) 119659.
39. T.K. Mukhopadhyay, S. Ghatak, H.S. Maiti, Ceram. Int. 35(4) (2009) 1493.
40. K. Snyder, Mineralogical and Microstructural Evolution Review, Current Understanding of the Parameters that Influence Hydraulic and Leaching Properties and Uncertainty Analysis of Cementitious Barriers, Savannah River National Laboratory, Aiken, SC, (2009)
41. A. Intiso, F. Rossi, A. Proto, et al., Rend. Fis. Acc. Lincei 32 (2021) 699.
42. G. Ulian, D. Moro, G. Valdrè, Appl. Clay Sci. 212 (2021) 106221.
43. A. Terzić, L. Pezo, N. Mijatović, J. Stojanović, M. Kragović, Lj. Miličić, Lj. Andrić, Constr. Build. Mater. 180 (2018) 199.
44. M. S. Malika, J. Build. Mater. Struct. 7 (2020) 119.
45. Z. He, A. Shen, Z. Lyu; Y. Li; H. Wu; W. Wang, Const. Build. Mater. 261 (2020) 119920.
46. S. Marince, D. Dumitras, C. Ghineţ, A. Fransolet, F. Hatert, M. Rondeaux, Canadian Mineral. 49(4) (2011) 1001.
47. Xu, P. Song, W.Cao, H. Li, J. Liang, Crystals 11 (2021) 936.
48. M. Merlini, G. Artioli, T. Cerulli, F. Cella, A. Bravo, Cem. Concr. Res. 38: 4 (2008) 477.

49. P. Gu, J.J. Beaudoin, J. Mater. Sci. 32 (1997) 3875.
50. L. Xu, P. Wang, G. De Schutter, Mat. Sci. Edit. 29 (2014) 751.
51. P. C. Hewlett (Ed) Lea's Chemistry of Cement and Concrete: 4th Ed, Arnold, 1998, ISBN 0-340-56589-6, p. 715
52. https://www.mindat.org/min-217.html
53. P. Dubreil, V.M. Sobolev, Refract. Indust. Ceram. 40 (3-4) (1999) 152.
54. T. Wala, B. Psiuka, J. Kubacki, K. Stec, J. Podwórny, Ceramics International 40 (2014) 5129.
55. D. Clarke, M. Dorais, B. Barbarin et al., J. Petrology 46:3 (2005) 441.
56. G. Kakali, S. Tsivilis, K. Kolovos et al., Cem. Concr. Compos. 27 (2005) 155.
57. D. Su, G. Yue, Q. Li, Y. Guo, S. Gao, L. Wang, Materials 12:9 (2019) DOI: 10.3390/ma12091510
58. Z. Lina, C. Xin, H. Dongshuai, G. Siyao, Const. Build. Mat. 155 (2017) 413.
59. M.J. Buerger, C. T. Prewitt. The crystal structures of wollastonite and pectolite. Proceedings of the National Academy of Sciences 47:12 (1961) 1884.

***Извод**: Филосиликатни минерал пирофилит се претежно користи у керамичкој индустрији јер показује високу ватросталност. Због своје термичке трансформације у мулит, пирофилит је стабилан на повишеним температурама, што га чини погодним минералним додатком за ватросталне необликоване материјале и различите керамичке обликоване производе. У овом раду пирофилит је коришћен као замена за 50 % глине у керамици и до 30 % замене за цемент у малтерима. Испитивана су физичко-механичка својства. Скупљање при печењу у керамици третираној на 1200 °C смањено је додавањем пирофилита. Пирофилит се понашао као додатни извор поцоланског материјала током хидратације цемента. Унутар микроструктуре формирао је микроарматуру у облику кристалне фолије, што је побољшало механичка својства малтера на бази обичног Портланд цемента, високоалуминатног цемента и мешаних цемента. Истраживањем је доказана ефикасност и погодност пирофилита који се користи као замена за глину у керамици и замена за цемент у малтерима.*

***Кључне речи**: минерални адитиви; синтеровање; одрживе сировине; инструменталне анализе.*